HHS Public Access

Author manuscript

J Struct Biol. Author manuscript; available in PMC 2019 March 01.

Published in final edited form as:

J Struct Biol. 2018 March ; 201(3): 237–246. doi:10.1016/j.jsb.2017.11.010.

Bone morphogenetic protein signaling through ACVR1 and BMPR1A negatively regulates bone mass along with alterations in bone composition

Ce Shi[a,b], **Gurjit S Mandair**[b], **Honghao Zhang**[b], **Gloria G. Vanrenterghem**[b], **Ryan Ridella**[c], **Akira Takahashi**[b], **Yanshuai Zhang**[b], **David H. Kohn**[b,d], **Michael D Morris**[c], **Yuji Mishina**[b,*], and **Hongchen Sun**[a,*]

[a]Department of Oral Pathology, School and Hospital of Stomatology, Jilin University; 1500 Qinghua Road, Changchun, 130000, China

[b]Department of Biologic and Materials Sciences, University of Michigan, School of Dentistry; 1011 N. University Avenue, Ann Arbor, MI 48109-1078, USA

[c]Department of Chemistry, University of Michigan; 930 N. University Avenue, Ann Arbor, MI 48108-1055, USA

[d]Biomedical Engineering College of Engineering, University of Michigan, MI 48109-2110, USA

Abstract

Bone quantity and bone quality are important factors in determining the properties and the mechanical functions of bone. This study examined the effects of disrupting bone morphogenetic protein (BMP) signaling through BMP receptors on bone quantity and bone quality. More specifically, we disrupted two BMP receptors, *Acvr1* and *Bmpr1a*, respectively, in *Osterix*-expressing osteogenic progenitor cells in mice. We examined the structural changes to the femora from 3-month old male and female conditional knockout (cKO) mice using micro-computed tomography (micro-CT) and histology, as well as compositional changes to both cortical and trabecular compartments of bone using Raman spectroscopy. We found that the deletion of *Acvr1* and *Bmpr1a*, respectively, in an osteoblast-specific manner resulted in higher bone mass in the trabecular compartment. Disruption of *Bmpr1a* resulted in a more significantly increased bone mass in the trabecular compartment. We also found that these cKO mice showed lower mineral-to-matrix ratio, while tissue mineral density was lower in the cortical compartment. Collagen crosslink ratio was higher in both cortical and trabecular compartments of male cKO mice. Our

Corresponding author: Yuji Mishina, University of Michigan, School of Dentistry, Department of Biologic and Materials Sciences, 1011 N. University Avenue, Ann Arbor, MI 48109-1078, Phone: +1-734-763-5579, Fax: +1-734-647-2110, mishina@umich.edu. Hongchen Sun, Jilin University, School and Hospital of Stomatology, Department of Oral Pathology, 1500 Qinghua Road, Changchun 130021, China, Phone: +86-0431-88796010, Fax: +86-0431-88975348, hcsun@mail.jlu.edu.cn.

Declaration of Interests

The authors report no conflicts of interest. The authors alone are responsible for the content and writing of the paper.

study suggested that BMP signaling in osteoblast mediated by BMP receptors, namely ACVR1 and BMPR1A, is critical in regulating bone quantity and bone quality.

Keywords

bone quantity; bone quality; micro-CT; Raman spectroscopy; BMP receptor; bone composition

1. Introduction

Bone is hierarchically structured to impart load-bearing functions and mechanical resilience to skeletal systems. Bone matrix is primarily composed of mineralized collagen fibrils stabilized by water with smaller amounts of noncollagenous proteins (NCPs), lipids, and proteoglycans (Stock, 2015). NCPs play critical roles at various stages of skeletal development, which translate through different hierarchical scales in bones to influence their compositional and mechanical properties (Morgan et al., 2015). NCPs include bone morphogenetic proteins (BMPs) (Derkx et al., 1998), which were originally identified as growth factors because they could induce bone and cartilage formation when implanted at ectopic sites (Urist, 1965).

By inhibiting BMP signaling, through the disruption or deletion of associated BMP receptors in mice, their effects on skeletal development have been studied. However, we previously found that tissue-specific deletion of BMP receptors (i.e. *Acvr1*, also known as *Alk2*, and *Bmpr1a*, also known as *Alk3*) in early differentiated osteoblasts resulted in an unexpected increase in bone mass (Kamiya et al., 2011; Kamiya et al., 2010; Kamiya et al., 2008a; Kamiya et al., 2008b). Conversely, we found that deletion of *Bmpr1a* in mature osteoblasts decreased bone mass in younger mutant mice (less than 6 months of age) but increased bone mass in older mutant mice (10 months of age) (Mishina et al., 2004). Thus, BMP signaling through BMP receptors appeared to regulate bone quantity in an age and a differentiation stage of osteoblasts-dependent manner in mice. This is one of the reasons we revisited phenotype analyses of osteoblast-specific disruption of *Bmpr1a* to compare phenotypes obtained from different Cre mice.

Micro-computed tomography (micro-CT) is used routinely to quantify bone mass and bone microarchitecture in small animal models, and the results can be tied in with structural and bone remodeling results obtained by histomorphometry. It is now well accepted that both bone mass and bone quality are factors in determining bone strength (Gourion-Arsiquaud et al., 2009). Bone quality affects biomechanical properties differentially depending on the amount and structure of bone matrix (i.e. mineral and collagen fiber) (Bouxsein, 2003). Therefore, additional techniques are often required to assess bone quality because it is an '*umbrella term*' used to describe a set of factors that are known to influence bone strength, such as bone microarchitecture, tissue composition, microdamage, morphology, and bone remodeling (Chappard et al., 2011; Jepsen, 2011). We and others have extensively studied alterations in bone mass in the BMP receptor mutant mice, however, whether and how BMP signaling regulates bone quality has yet to be fully understood.

Raman spectroscopy is increasingly being used to characterize bone tissue composition and thus contributes towards the understanding of how defective genes or proteins impact bone quality (Mandair and Morris, 2015). Tissue-level spectroscopic measures of bone quality include mineral-to-matrix ratio (MMR), mineral crystallinity, carbonate-to-phosphate ratio (CPR), and collagen crosslink ratio. MMR provides information on the degree of mineral within a given volume of bone matrix analyzed and is positively correlated with ash weight (Boskey and Mendelsohn, 2005; Taylor et al., 2017). Whereas, mineral crystallinity and CPR are measures of bone mineral crystallite size and/or lattice perfection (Awonusi et al., 2007; Freeman et al., 2001). More recently, CPR has been related to bone remodeling in a correlative bone histomorphometry study (Isaksson et al., 2010). Changes in bone matrix quality is often accompanied by changes in collagen amide I secondary structure. For instance, the amide I non-reducible to reducible collagen-linking ratio has been used as measures of collagen maturity, which increases with age and bone fragility (Boskey and Mendelsohn, 2005; Gong et al., 2013).

Recently, we reported alterations in bone quality, such as an increased MMR, in our *Bmpr1a* conditional knockout mice (Zhang et al., 2016). In that report, we used a tamoxifen (TM) - inducible Cre under the control of a 3.2-kb mouse pro-collagen I promoter (*Col1*-CreER™). We induced the Cre activity by injecting tamoxifen intraperitoneally. Here, we re-investigate BMP signaling function in bone homeostasis using a different Cre-loxP system, *Osterix*-Cre (Tet-off) (Rodda and McMahon, 2006), for the following reasons; (1) although the tamoxifen inducible method is powerful to study stage-specific function of BMP signaling, it has an intrinsic concern, since tamoxifen treatment affects bone mineral density (Powles et al., 1996), and more importantly, (2) evidence shows that specific disruption of *Bmpr1a* in osteoblasts using different Cre drivers, i.e. *Og2*-Cre (Mishina et al., 2004), *Col1*-Cre (Kamiya et al., 2008b; Zhang et al., 2016), *Dmp1*-Cre (Kamiya et al., 2016; Lim et al., 2016), leads to different bone phenotypes in mice. Comparisons of changes in bone quality between mutant mice using Cre with different osteogenesis stage-specificity would provide more accurate information on how BMP signaling influences bone quality. This is a relevant consideration based on our recent report regarding bone phenotype found in *Bmpr1b* global mutant mice (Shi et al., 2016). Bone marrow cells (an earlier stage during osteogenic differentiation) from *Bmpr1b* mutant mice show more drastic changes than preosteoblasts (a later stage during osteogenic differentiation) from *Bmpr1b* mutant mice (Shi et al., 2016); demonstrating evidence that function of BMP signaling is different depending on the stage of osteogenesis.

In this study, to avoid the effects of tamoxifen on bone, and to examine how bone is affected when *Bmpr1a* is ablated at a much earlier stage during osteoblast differentiation, we introduced another inducible Cre system, *Osterix*-Cre (Tet-off) (Rodda and McMahon, 2006) to disrupt *Bmpr1a* (A3cKO). We also disrupt another type 1 BMP receptor, *Acvr1* (A2cKO), to compare bone phenotypes. *Osterix* is the direct downstream target of *Runx2*, and *Runx2* is the first transcription factor required for determination of the osteoblast lineage from mesenchymal stem cells towards preosteoblast (Komori, 2010). Thus, BMP receptors are disrupted in preosteoblast and later stage. To determine the roles of ACVR1 and BMPR1A in bone remodeling, we activated the Cre activity after weanling stage, and harvested the bones at 3 months of age for further analyses.

Here, we report a detailed quantitative assessment of cortical and trabecular compartments in femora from both male and female *Acvr1* and *Bmpr1a* cKO mice using micro-CT and histomorphometry. Raman spectroscopy analyses were also performed with the aim of understanding how the deletion of BMP receptors influenced bone quality. Furthermore, correlations between micro-CT and Raman spectroscopic parameters were also examined to clarify the relationship between bone or tissue mineral density with bone tissue composition.

2. Materials and Methods

2.1. Generation of conditional knockout (cKO) mice

To generate *Acvr1* or *Bmpr1a* conditional knockout (cKO) mice, mice homozygous for both the conditional allele for the receptors and the *ROSA26*-Cre reporter (*Acvr1* fx/fx: *R26R*/*R26R* or *Bmpr1a* fx/fx: *R26R*/*R26R*) (Kaartinen and Nagy, 2001; Mishina et al., 2002; Soriano, 1999) were bred with mice heterozygous for the conditional allele carrying *Osterix*-Cre (*Acvr1* fx/+: *Osx*-Cre or *Bmpr1a* fx/+: *Osx*-Cre) (Rodda and McMahon, 2006). To suppress Cre activity before weanling, designated breeders were fed a diet containing 625 mg/kg doxycycline (Harlan, USA) to deliver a daily dose of 2–3 mg/mouse of doxycycline according to manufacturer's instruction. Cre activity was activated after the weanling stage by switching from doxycycline chow to regular rodent diet. Mice genotyped *Acvr1* fx/fx: *Osx*-Cre: *RS*/+ and *Bmpr1a* fx/fx: *Osx*-Cre: *RS*/+ were designated as *Acvr1* conditional knockout (A2cKO) and *Bmpr1a* conditional knockout (A3cKO), respectively. Mice genotyped negative for *Osx*-Cre were used as control (con). It is known that the *Osx*-Cre knock-in allele itself causes hypermineralization, but dox chow treatment during pregnancy can rescue this phenotype (Davey et al., 2012; Wang et al., 2015). Control and cKO mice were sacrificed at 3 months of age. All animal experiments in this study were approved by the Institutional Animal Care and Use Committee (UCUCA) at the University of Michigan.

2.2. Micro-computed tomography (micro-CT)

Left femora were embedded in 1% agarose (Luderer et al., 2008) and placed in a 19 mm diameter tube and scanned over the entire length of the bones using a micro-CT system (μCT100 Scanco Medical, Bassersdorf, Switzerland). Scan settings were: voxel size 10 μm, medium resolution, 70 kVp, 114 μA, 0.5 mm AL filter, and integration time 500 ms. A 0.5 mm region of trabecular compartment was analyzed immediately below the growth plate using a fixed global threshold of 26% (260 on a grayscale of 0–1000, or 569 mg HA/ccm); and a 0.3 mm region of cortical compartment around the midpoint was analyzed using a fixed global threshold of 36% (360 on a grayscale of 0–1000, or 864 mg HA/ccm). Trabecular bone volume fraction (BV/TV), trabecular thickness (Tb. Th), trabecular number (Tb. N), trabecular separation (Tb. Sp), cortical bone volume fraction (BV/TV), cortical porosity (1-BV/TV), bone mineral density (BMD) and tissue mineral density (TMD) were analyzed using the manufacturer's evaluation software.

2.3. X-gal staining

Tibiae were dissected free of soft tissues, and fixed in 4% paraformaldehyde (PFA) for 10 min on ice. Then the fixed bones were rinsed with PBS, and stained with X-gal solution (containing 1 mg/ml X-gal, 5 mM potassium hexacyanoferrate, 5 mM potassium

hexacanoferrate, 0.1% sodium deoxycholate, 2% NP-40, 2 mM $MgCl_2$ in 0.1M sodium phosphate buffer) at 37°C overnight.

2.4. Histology and histomorphometry

Left femora and the X-gal stained tibiae were further fixed in 4% PFA, decalcified with 10% EDTA, and embedded in paraffin. Longitudinal sections were made at 7 μm, and femoral sections were stained for hematoxylin and eosin (HE) and tartrate-resistant acid phosphatase (TRACP), and X-gal stained tibia sections were counterstained with diluted eosin.

Static histomorphometry was performed on sections taken from the femora. Histomorphometry measurements were made in a blinded, nonbiased manner using Image J (1.49P). Regions of interest (ROIs) were confined to the secondary spongiosa and restricted to a square area between 300–1400 μm proximal to the growth plate of the distal femora. Parameters were measured according to the Report of the American Society of Bone and Mineral Research Histomorphometry Nomenclature Committee (Dempster et al., 2013).

2.5. Embedding

Right femora were dehydrated in graded ethanol, defatted in Clear-Rite 3 (Richard-Allen Scientific, Kalamazoo, MI), and then embedded in polymethylmethacrylate (PMMA, Koldmount Cold Mounting Kit, Mager Scientific). The embedded specimens were sectioned at low speed using a diamond wafering blade under constant irrigation. Transverse sections were made at middle (mid-diaphysis) and distal (0.5 mm above distal growth plate) femora to a thickness of approximately 2 mm each. The sections were sequentially polished using wet silicon carbide abrasive discs of grit 400, 1200, 2400 and 4000 (Buehler, Lake Bluff, IL).

2.6. Raman spectroscopy

The Raman microscope was constructed locally as described previously (Rux et al., 2017) but was fitted with a 785 nm diode laser (Innovative Photonics Solutions, Monmouth Junction, NJ) and a 25 μm slit to give a spectral resolution of ~4 cm^{-1}. The excitation laser was spot-focused to give ~28 mW of laser power at the sample when focused through a 20×/0.75 *NA* objective (S Fluor, Nikon Instruments, Inc., Melville, NY). Transverse femoral mid-shaft sections were mounted onto a custom-made rotating platform to ensure that the irradiated site was aligned parallel to the cortical bone surfaces. For cortical compartments, areas 10–20 μm from the periosteum and endosteum were defined as our measurement sites at each of the four bone quadrants. A total of 8 cortical spectra were acquired from each specimen using a spectral accumulation cycle time of 6 mins (2 × 3 mins). For trabecular compartments, 4–6 spectra were taken from the plate-like structures within the central portion of distal transverse femoral sections.

All Raman spectroscopic data were calibrated and processed in MATLAB® software using locally written scripts described elsewhere (Esmonde-White et al., 2011; Rux et al., 2017). The script included an automated '*derivative minimization*' procedure to remove spectral interference from PMMA (Banerjee and Li, 1991), while an '*adaptive min-max*' polynomial fitting procedure (3rd order, constrained) was used to correct for background tissue

fluorescence (Cao et al., 2007). All spectra were imported into GRAMS/AI® software for baseline correction and normalization against the symmetrical ν_1 phosphate band at ~959 cm^{-1} (ν_1PO_4). For optimal curve-fitting, second derivative and constrained Gaussian deconvolution functions were applied to the following spectral regions: 830–904 cm^{-1} (854, 875, 895 cm^{-1}); 901–990 cm^{-1} (922, 943, 959 cm^{-1}); 1010–1115 cm^{-1} (1019, 1027, 1043, 1070, 1087, 1100 cm^{-1}); and 1540–1716 cm^{-1} (1545, 1561, 1579, 1592, 1604, 1626, 1641, 1660, 1681, 1702 cm^{-1}). Additional Raman bands relevant to bone were also identified: symmetrical ν_1 carbonate band at ~1070 cm^{-1} (ν_1CO_3); and amide I sub-bands at ~1660 cm^{-1} (non-reducible crosslinks) and ~1681 cm^{-1} (reducible crosslinks) (Gong et al., 2013). The following relative intensity ratiometric parameters were calculated: mineral-to-matrix ratio (MMR, 959 cm^{-1}/(854+875) cm^{-1}); carbonate-to-phosphate ratio (CPR, 1070 cm^{-1}/959 cm^{-1}); and collagen crosslink ratio (1660 cm^{-1}/1681 cm^{-1}). The mineral crystallinity parameter was the inverse of the full-width at half maximum (1/FWHM) of the Gaussian-fitted ν_1PO_4 band at 959 cm^{-1}. In this study, cortical measurements from the femoral mid-shaft were averaged to provide a more representative mean value for each specimen. Similarly, trabecular measurements from the distal region of the femora sections were also averaged.

2.7. Statistical analysis

All calculations and statistical analyses were performed in SPSS Statistics Software for Windows (IBM SPSS Version 22, IBM Corp., NY). The results were expressed as means ± standard deviations. The numbers of specimens used for each experiment are found in the figure legends. One-way analysis of variance (ANOVA) with Bonferroni post-hoc tests were used to evaluate the statistical differences between the 3 genotype groups. The details of the power analyses (80%, a = 0.05) has been described elsewhere (Rux et al., 2017). In all tests, $p < 0.05$ was considered to be statistically significant. Select cortical Raman spectroscopic and cortical micro-CT measurements from all three groups (control, A2cKO, and A3cKO mice) were pooled by gender prior to linear regression analysis. Correlations between cortical MMR and cortical bone mineral density (BMD), and cortical MMR and cortical tissue mineral density (TMD) were obtained and R^2 values were reported.

3. Results

3.1. BMP receptors are disrupted in osteoblasts

To determine the efficiency of the deletion of BMP receptors, we introduced the *ROSA26*-Cre reporter allele to the cKO mice and performed X-gal staining in tibiae of 3-month-old mice. X-gal stained blue cells indicated the expression of *LacZ*, suggesting that recombination occurred at the floxed sites. Control mice which were Cre (−) showed no X-gal stained cells as expected (Fig. 1A). For both A2cKO and A3cKO bones, LacZ positive cells were seen along the bone surface, as well as in the bone matrix, which were supposed to be osteoblasts and osteocytes, respectively (Fig. 1A). Gene deletion efficiency was defined as number of LacZ positive cells divided by total cell number in osteoblast lineage. Figure 1B showed that gene deletion efficiencies were quite high in both cKO bones (> 80%), and there was no difference between A2cKO and A3cKO. Taken together, these data

suggest that BMP receptors were specifically disrupted in osteoblast lineage with high efficiencies in our cKO mouse models.

3.2. Osteoblast-specific disruption of Acvr1 and Bmpr1a results in higher bone mass

Micro-CT images showed both A2cKO and A3cKO mice had higher bone mass in trabecular compartments of femora, and A3cKO mice had more bone mass than A2cKO in the trabecular compartment at 3 months of age in both males and females (Fig. 2A and Fig. 3A, respectively). In cortical compartment of male mice, there was no difference in BV/TV or cortical porosity among the controls, A2cKO and A3cKO (Fig. 2B and 2C). There was no difference in cortical BMD among the three groups, however, A3cKO is lower in tissue mineral density (TMD) (5.5% and 4.6% decrease compared with control and A2cKO, respectively, $p < 0.01$) (Fig. 2D). In the trabecular compartment of male mice, A2cKO showed a 59% increase in BV/TV compared with control ($p < 0.05$), and A3cKO showed 1.7-fold and 67% increase in BV/TV compared with control and A2cKO, respectively (Fig. 2E, $p < 0.01$). Correspondingly, A2cKO showed a 41% increase in BMD compared with control ($p < 0.01$), and A3cKO showed 1.2-fold and 57% increase in BMD compared with control and A2cKO ($p < 0.01$), respectively (Fig. 2F). The increased bone mass observed in cKO mice was due to the increase in both the trabecular number (Tb. N) and trabecular thickness (Tb. Th). For Tb. N, A2cKO showed 21% increase compared with control ($p < 0.05$), and A3cKO showed 26% increase compared with control (Fig. 2G, $p < 0.01$). For Tb. Th, A3cKO had 1.3-fold and 83% increase compared with control and A2cKO, respectively (Fig. 2H, $p < 0.01$). Thus, for Tb. Sp, A2cKO showed 25% decrease compared with control ($p < 0.01$), and A3cKO showed 45% decrease compared with control (Fig. 2I, $p < 0.01$) and 27% decrease tendency compared with A2cKO (Fig. 2I, $p = 0.05$). For 3-month old female mice, we found basically similar changes in alterations for those parameters (Fig. 3).

To determine the histological changes in the femora, several static histomorphometric parameters were examined. Since there was no gender difference in the parameters tested by micro-CT, we performed static histomorphometry only in male mice. Consistent with but even more significant than results obtained by micro-CT, bone areas were 3-fold and 7.7-fold higher in male A2cKO and A3cKO, respectively, compared with control ($p < 0.01$), and that A3cKO had 2.5-fold higher bone area compared with A2cKO ($p < 0.01$) (Fig. 4A and 4B). Both cKO had 67% increase of Tb. N compared with control (Fig. 4C, $p < 0.01$ and $p < 0.05$, respectively). Tb. Th was increased by 82% and 5.5-fold in A2cKO and A3cKO, respectively, compared with control ($p < 0.01$), and A3cKO had 3-fold increase in Tb. Th. compared with A2cKO ($p < 0.05$) (Fig. 4D). Thus, trabecular separation (Tb. Sp) was decreased by 56% and 80% in A2cKO and A3cKO, respectively, compared with control ($p < 0.01$), and A3cKO was further decreased by 55% compared with A2cKO ($p < 0.01$) (Fig. 4E). In terms of osteoblast number (N. Ob) and osteoblast surface (Ob. S), there were no differences between control and A2cKO, while A3cKO showed decreased N. Ob and Ob. S compared with A2cKO ($p < 0.05$) and decreased tendency compared with control ($p = 0.12$) (Fig. 4F and 4G). Besides a decrease of osteoclast number (N. Oc) in A3cKO compared with control ($p < 0.05$), both cKO showed decreased tendency in N. Oc, osteoclast surface (Oc. S) and eroded surface (ES), compared with control, and A3cKO showed decreased tendency compared with A2cKO (Fig. 4H–4J).

3.3. Conditional disruption of Acvr1 or Bmpr1a alters bone composition

Bone tissue composition of cortical and trabecular compartments of male and female femoral transverse sections were examined by Raman spectroscopy. For male mice, no significant differences in mineral crystallinity between the cKOs and the control mice were found for either the cortical (Fig. 5A leftmost panel) or trabecular compartments (Fig. 5B leftmost panel). Both A2cKO and A3cKO male mice had significantly lower mineral-to-matrix ratios (MMRs) in the cortical compartment (Fig. 5A second panel, 14% and 15% decrease, respectively, $p < 0.01$) compared to the control. In contrast, no significant differences in the MMRs between the trabecular compartments of the male cKOs and the control were found (Fig. 5B second panel), compared with the control. Changes in cortical MMRs (Fig. 5A and Fig. 6A) were more consistent with changes in TMD than with BMD (Fig. 2D and 3D). For the cortical compartments, male A2cKO and A3cKO mice had a significant increase in collagen crosslink ratios, compared to the control mice (Fig. 5A, third panel, 9% and 12 increase, respectively, $p < 0.05$ and $p < 0.01$, respectively), while only A3cKO male mice exhibited 13% increase in collagen crosslink ratio in the trabecular compartment compared to control mice (Fig. 5B third panel, $p < 0.01$). No significant differences in the carbonate-to-phosphate ratio (CPR) were found between cKOs and the control mice in either of the cortical and trabecular compartments (Fig. 5A and 5B, rightmost panels).

When male and female mice were compared, changes in MMRs and collagen crosslink ratio parameters in the cortical and trabecular compartments showed similar tendencies to those found in male cKOs and control mice (Fig. 6 vs. Fig. 5). When female cKO mice were examined, the cortical compartment of the A3cKO mice exhibited a decrease in MMR compared to the control (Fig 6A, 18% decrease, second panel, $p < 0.01$). There were no differences between control and cKOs in terms of mineral crystallinity (Fig. 6A and 6B, leftmost panels), collagen crosslink ratio (Fig. 6A and 6B, third panels), or CPR (Fig. 6A and 6B, rightmost panels).

To determine correlations between Raman spectroscopy and micro-CT parameters, measurements from all three groups (control, A2cKO, and A3cKO mice) were pooled by gender and linear regression analyses were performed between the following parameters: TMD *vs.* MMR; and BMD *vs.* MMR. As shown in Fig. 7, both TMD and BMD from male cortical compartments showed linear correlations with MMR, but TMD *vs.* MMR showed higher correlations than BMD *vs.* MMR (R^2 values of 0.5009 and 0.2606, respectively, $p < 0.05$ and $p < 0.01$, respectively) (Fig. 7A and 7B). While in females, only TMD from cortical compartments showed linear correlations with MMR (R^2 value of 0.5108, $p < 0.01$) (Fig. 7C and 7D).

4. Discussion

In this study, we demonstrated that osteoblast-specific deletions of *Acvr1* and *Bmpr1a* using *Osx*-Cre resulted in a higher bone mass in the trabecular compartment, together with higher collagen crosslink ratio, and lower MMR in the cortical compartments in male cKO mice at the weanling stage. These results demonstrate that BMP signaling mediated by ACVR1 and BMPR1A negatively regulate bone mass in *Osterix*-expressing cells. Moreover, we found

that the changes in trabecular bone volume fraction and BMD in *Bmpr1a* cKO mice were more significant when compared to those in *Acvr1* cKO mice. Our findings indicate a more critical role of BMPR1A in regulating bone quantity and bone quality than ACVR1, especially in the trabecular compartment, when each receptor is disrupted at a stage when *Osterix* is started to be expressed, which is earlier than the stage when *Col1* is expressed. We also found gender-specific phenotypes in bone quality in our cKO mice, while bone quantity was similarly affected in both genders.

Our findings that BMP receptors, ACVR1 and BMPR1A, negatively regulated bone mass in *Osterix*-expressing cells were similar with, but not identical to our and others' previous studies using other Cre-drivers specific for osteoblast lineage (Kamiya et al., 2011; Kamiya et al., 2010; Kamiya et al., 2008a; Kamiya et al., 2008b; Kamiya et al., 2016; Lim et al., 2016; Mishina et al., 2004). We have previously shown that deletion of *Bmpr1a* using *Og2*-Cre affects bone remodeling in an age-dependent manner (Mishina et al., 2004). At younger age (less than 6 months of age), bone mass is lower in the cKO; however, bone mass is higher in older cKO mice (at 10 months of age). We also found that deletion of *Bmpr1a* using a 3.2-kb *Col1*-CreER resulted in a higher trabecular bone mass at both postnatal stages (3 and 22 weeks of age) (Kamiya et al., 2010; Kamiya et al., 2008b) and embryonic stage (E18.5) (Kamiya et al., 2008a). We found that the mutant osteoblasts fail to support osteoclastogenesis resulting in an imbalance between bone formation and resorption (Kamiya et al., 2008a). In addition, deletion of *Acvr1* using the same 3.2-kb *Col1*-CreER results in a higher bone mass at embryonic stage (E18.5) and adult stage (postnatal day 21) (Kamiya et al., 2011).

In this current study, we used an inducible *Osx*-Cre (Tet-off) to activate the Cre activity after weanling stage, and harvested bones at 3 months of age. Consistent with *Col1*-CreER but opposite to *Og2*-Cre systems, we found increased bone mass in the trabecular compartment of both A2cKO and A3cKO femora, and A3cKO showed a more markedly increased bone mass compared with A2cKO (Fig. 2, Fig. 3 and Fig. 4). In *Col1*-CreER system, disruption of *Acvr1* exhibits the same bone phenotypes as that of *Bmpr1a* (Kamiya et al., 2011; Kamiya et al., 2008b). The current result not only confirmed that ACVR1 and BMPR1A in osteoblasts negatively regulate bone mass, but also suggested that BMPR1A may play a more significant role than ACVR1 in maintenance of bone homeostasis. *Osterix* is expressed in preosteoblasts (Komori, 2010), and *type I Collagen* is one of the target genes of *Osterix* (Nakashima et al., 2002), whereas *Og2* (*Osteocalcin gene 2*) is expressed in mature osteoblasts (Komori, 2010). *Osx*-Cre is expressed in committed osteoblast progenitors in a manner following that of endogenous *Osterix* (Nakashima et al., 2002; Rodda and McMahon, 2006). For 3.2-kb *Col1*-CreER, when activate Cre at E13.5, the pups at E14.5 displayed a staining pattern similar to *Osx*-Cre, whereas *Osx*-Cre was expressed earlier in development than *Col1* (3.2 kb)-CreER (Maes et al., 2010). *Og2*-Cre is expressed in mature/differentiated osteoblasts (Dacquin et al., 2002). Taken together, our previous and current study indicated that deletion of *Bmpr1a* at different stages of osteoblast differentiation resulted in different phenotypes in bone.

Immature osteoblast lineage cells exhibit increased osteoclastogenic induction, compared with mature osteoblasts (Li et al., 2010). Since deletion of BMP receptors in osteoblasts

resulted in decreased activities of both bone formation and bone resorption (Kamiya et al., 2010; Kamiya et al., 2008b), it is possible to speculate that upon deletion of *Bmpr1a* in mature osteoblasts (i.e. *Og2*-Cre) exert a minimal impact on osteoclastogenesis because osteoblasts can communicate with osteoclasts before differentiation to mature osteoblasts. In contrast, in the case of deletion of *Bmpr1a* in immature osteoblasts (i.e. 3.2-kb *Col1*-CreER and *Osx*-Cre), osteoclastogenesis is more impacted resulting in increased bone mass despite the lower bone formation rate.

In addition to bone mass, bone quality was also examined between the controls and cKO mice. In this study, Raman spectroscopy was used to examine the following four bone tissue compositional measures of bone quality: MMR, mineral crystallinity, CPR, and collagen crosslink ratios. The effect of the conditional deletion of BMP receptors on each of these bone compositional parameters will be discussed in turn.

First, if we compare between male and female, there were some differences, i.e. MMR, collagen crosslink ratio, and BMD vs. MMR correlation (Fig. 5, Fig. 6 and Fig. 7, respectively). The possible explanations for these gender dependent phenotypes are: (1) the difference in hormonal regulation between the genders (Nilsson et al., 1994); (2) the difference in adaptation between the genders, e.g. bones in different genders respond differently to exercise (Wallace et al., 2009; Wallace et al., 2007).

MMRs were found to be reduced in the cortical compartment of A2cKO and A3cKO male mice compared to control mice (Fig. 5A), including the cortical compartment of female A3cKO mice (Fig. 6A). Similar reductions in cortical MMRs had also been reported in the long bones of *Bmp*-2 knockout (*Osx*-Cre) mice (McBride et al., 2014). However, cortical MMRs were only significantly reduced in the humeri of 6-month male and female *Bmp2* fl/fl cKO mice and not in the femur of 3-month old male *Bmp2* fl/fl cKO mice. More recently, we found that conditional deletion of *Bmpr1a* using a 3.2-kb *Col1*-CreER (induce Cre activity by injecting tamoxifen between 16 weeks and 20 weeks of age, and dissect the mice at 22 weeks of age) resulted in a significant increase in MMRs in the trabecular compartments, but not in the cortical compartments of femora from cKO (Zhang et al., 2016). The later results were obtained using *Col1*-CreER mice as opposed to *Osterix*-Cre (Tet-off) mice used in the current study. The discrepancy in MMRs (and other potential bone tissue compositional parameters) may be caused by differences in the timing of Cre-induced recombination between different promoters (*Osx*-Cre is activated at more immature stage of osteoblastic differentiation as discussed above). An alternative but not exclusive possibility is the difference in the period of bone remodeling after induction of Cre recombination (induced at 16 weeks to harvest at 22 weeks of age for 3.2-kb *Col1*-CreER *vs*. induced at 3 weeks to harvest at 12 weeks of age for *Osx*-Cre). This possibility is supported, in part, by our study which shows age-dependent phenotypes using an *Mx1*-Cre transgenic line to disrupt *Bmpr1a* in an age-specific manner (Zhang et al., 2003). Thirdly, it is also possible that tamoxifen treatment, which is involved in generating *Col1*-CreER mice, may also in part account for some of these differences because it can induce bone loss (Powles et al., 1996). How tamoxifen affects bone quality is not clearly understood, but it is possible that tamoxifen may affect bone quality differently when BMP signaling is lowered in osteoblasts.

When cortical MMRs from control, A2cKO, and A3cKO male mice were regressed against corresponding bone or tissue mineral density measurements, the correlations were stronger with tissue mineral density (TMD) than with bone mineral density (BMD). The moderate linear correlations found between cortical TMD and MMR were most likely attributed to regressing between two tissue level properties that were less sensitive towards void spaces and other parameters that impact volume measures. BMD predominately reflects changes in structural level properties and therefore unlike TMD would be more sensitive towards bone volume effects. This would explain why more significant differences between the trabecular compartments of cKO and control mice were found using BV/TV and BMD variables (Fig 2E–F and Fig. 3E–F). Although, MMR is not a volumetric-based measurement, correlations between Raman (or infrared) spectroscopic MMRs and bone or tissue density measurements have widely been reported using either TMD or BMD (Gollwitzer et al., 2015; Miller et al., 2007; Turunen et al., 2011). However, studies have also shown that tissue-level changes in trabecular MMRs are not always mirrored by corresponding changes in BMD (Burket et al., 2013; Turunen et al., 2013) and that changes in cortical MMRs between experimental groups may be more statically significant compared to between-group BMD measurements (Inzana et al., 2013; Iwasaki et al., 2011). In the present study, the MMRs obtained for the trabecular compartments of male and female cKO mice exhibited reduced tendencies (Fig. 5B and Fig 6B) despite the fact that BMDs were significantly higher in these same mice (Fig. 2F and Fig. 3F). Experimental differences between Raman and micro-CT techniques, as well as the intrinsic heterogeneity and high turnover of trabecular may also account for some of these conflicting results.

In regard to bone mineral crystallinity and CPRs, no significant differences between the cKOs and the control mice were found. However, the lower mineral crystallinity values displayed by the cortical compartments of male cKO mice were mirrored by corresponding high CPRs (Fig. 5A). Decreased mineral crystallinity and increased CPRs would indicate the presence of immature bone mineral crystallites (Cornelis Klein, 2007). This result would be consistent with our micro-CT (Fig. 2 and Fig. 3) and MMR (Fig. 5 and Fig. 6) data for A2cKO and A3cKO male mice. Both cKO mice exhibited higher bone mass, lower TMD, and lower MMR compared to control mice, which again would indicate that the bone formed was immature and not well mineralized.

Although, reduced MMR found in the trabecular compartment of male A3cKO mice could be explained by reduced Ob. S/BS when compared to A2cKO mice, the relationship between bone histomorphometric and Raman spectroscopic measures of bone metabolism is not always straightforward. Indeed, a recent correlative FTIR spectroscopy and bone histomorphometric study found that reduced Ob. S/BS and Oc. S/BS activity were correlated with increased CPRs (Isaksson et al., 2010). In our current study, male A3cKO mice, the cKO with the lowest Oc. S/BS activity, exhibited the highest CPR value. This result suggests that the CPR parameter in this study was more related with the maturity of the bone mineral crystallites than with histomorphometric measures of bone metabolism.

Changes in mineralization patterns have often been accompanied by changes in bone collagen matrix properties. In this study, the intensity ratio of the Raman spectroscopic amide I non-reducible to reducible sub-bands were used as a surrogate measure of collagen

crosslink ratio or collagen maturity (Gong et al., 2013). Collagen crosslink ratio was found to be elevated in both cortical and trabecular compartment of male A3cKO mice. In a previous study involving *Col1*-CreER mice, collagen crosslink ratio was increased in the trabecular compartment of male cKO mice, and that the result coincided with increased levels of mature crosslinks as measured by HPLC (Zhang et al., 2016). In addition, A2cKO male mice exhibited an increase in collagen crosslink ratio only in cortical compartment, but not in trabecular compartment, compared with control (Fig. 5). The cortical compartment-specific increase in collagen crosslink ratio found in this current study could be attributed to altered bone matrix turnover, which had previously been reported in another study involving cKO of *Bmpr1a* mice driven by *Col1*-CreER (Iura et al., 2015). In that study, the loss of *Bmpr1a* signaling resulted in an increase in cortical collagen fibril diameters, which was attributed to the slower turnover of bone matrix due to reduced osteoclastogenesis. The notable absence of a similar increase in the collagen crosslink ratio within the cortical compartment of female mice (this study, Fig. 5 and Fig. 6) suggests that gender could also potentially modulate the effect of reduced BMP signaling on bone collagen matrix properties, while gender plays a minimal role in determining bone mass (Fig. 2 and Fig. 3).

5. Conclusions

In conclusion, our study found that conditional deletion of *Acvr1* or *Bmpr1a* specifically in early differentiated osteoblasts resulted in higher bone mass in the trabecular compartment, together with tissue-level compositional changes in both cortical and trabecular compartments. Our study suggested that BMP signaling in osteoblasts is an important factor in determining bone mass and bone quality. Further studies are required to understand how genetic deletion of BMP receptors regulates bone mechanical properties and whether these changes are correlated with subsequent changes in bone tissue composition.

Acknowledgments

We thank Jessica Deese and Dr. Erin McNerny for their technical support, Drs. Fei Liu and Rhima Coleman for their critical reading. This work was supported by grants from the National Institutes of Health (R01DE020843 to YM; U01DE023771 to DHK), the National Natural Science Foundation of China (No. 81320108011 to HS; No. 81600843 to CS; No. 81500820 to Chen Li), the National Key Research and Development Program of China 2016YFC1102800 to HS, and the Fundamental Research Funds for the Central Universities and JLU Science and Technology Innovative Research Team 2017TD-11 to HS. Research reported in this publication was supported in part by a core grant from the National Institutes of Arthritis and Musculoskeletal and Skin Diseases of the National Institutes of Health (P30 AR069620 to Karl Jepsen, PI; David H. Kohn, Core Director). The micro-CT core at the School of Dentistry, University of Michigan is funded in part by NIH/NCRR S10RR026475-01.

References

Awonusi A, Morris MD, Tecklenburg MM. Carbonate assignment and calibration in the Raman spectrum of apatite. Calcified tissue international. 2007; 81:46–52. [PubMed: 17551767]

Banerjee S, Li D. Interpreting multicomponent infrared spectra by derivative minimization. Applied spectroscopy. 1991; 45:1047–1049.

Boskey A, Mendelsohn R. Infrared analysis of bone in health and disease. Journal of biomedical optics. 2005; 10:031102. [PubMed: 16229627]

Bouxsein ML. Bone quality: where do we go from here? Osteoporos Int. 2003; 14(Suppl 5):S118–127. [PubMed: 14504716]

Burket JC, Brooks DJ, MacLeay JM, Baker SP, Boskey AL, van der Meulen MC. Variations in nanomechanical properties and tissue composition within trabeculae from an ovine model of osteoporosis and treatment. Bone. 2013; 52:326–336. [PubMed: 23092698]

Cao A, Pandya AK, Serhatkulu GK, Weber RE, Dai H, Thakur JS, Naik VM, Naik R, Auner GW, Rabah R, Freeman DC. A robust method for automated background subtraction of tissue fluorescence. Journal of Raman Spectroscopy. 2007; 38:1199–1205.

Chappard D, Basle MF, Legrand E, Audran M. New laboratory tools in the assessment of bone quality. Osteoporosis international : a journal established as result of cooperation between the European Foundation for Osteoporosis and the National Osteoporosis Foundation of the USA. 2011; 22:2225–2240.

Cornelis Klein, BD. Manual of Mineral Science. 23. John Wiley & Sons; 2007.

Dacquin R, Starbuck M, Schinke T, Karsenty G. Mouse alpha1(I)-collagen promoter is the best known promoter to drive efficient Cre recombinase expression in osteoblast. Developmental dynamics : an official publication of the American Association of Anatomists. 2002; 224:245–251. [PubMed: 12112477]

Davey RA, Clarke MV, Sastra S, Skinner JP, Chiang C, Anderson PH, Zajac JD. Decreased body weight in young Osterix-Cre transgenic mice results in delayed cortical bone expansion and accrual. Transgenic research. 2012; 21:885–893. [PubMed: 22160436]

Dempster DW, Compston JE, Drezner MK, Glorieux FH, Kanis JA, Malluche H, Meunier PJ, Ott SM, Recker RR, Parfitt AM. Standardized nomenclature, symbols, and units for bone histomorphometry: a 2012 update of the report of the ASBMR Histomorphometry Nomenclature Committee. Journal of bone and mineral research : the official journal of the American Society for Bone and Mineral Research. 2013; 28:2–17.

Derkx P, Nigg AL, Bosman FT, Birkenhager-Frenkel DH, Houtsmuller AB, Pols HA, van Leeuwen JP. Immunolocalization and quantification of noncollagenous bone matrix proteins in methylmethacrylate-embedded adult human bone in combination with histomorphometry. Bone. 1998; 22:367–373. [PubMed: 9556137]

Esmonde-White FW, Esmonde-White KA, Morris MD. Minor distortions with major consequences: correcting distortions in imaging spectrographs. Applied spectroscopy. 2011; 65:85–98. [PubMed: 21211158]

Freeman JJ, Wopenka B, Silva MJ, Pasteris JD. Raman spectroscopic detection of changes in bioapatite in mouse femora as a function of age and in vitro fluoride treatment. Calcified tissue international. 2001; 68:156–162. [PubMed: 11351499]

Gollwitzer H, Yang X, Spevak L, Lukashova L, Nocon A, Fields K, Pleshko N, Courtland HW, Bostrom MP, Boskey AL. Fourier Transform Infrared Spectroscopic Imaging of Fracture Healing in the Normal Mouse. Journal of spectroscopy. 2015:2015.

Gong B, Oest ME, Mann KA, Damron TA, Morris MD. Raman spectroscopy demonstrates prolonged alteration of bone chemical composition following extremity localized irradiation. Bone. 2013; 57:252–258. [PubMed: 23978492]

Gourion-Arsiquaud S, Faibish D, Myers E, Spevak L, Compston J, Hodsman A, Shane E, Recker RR, Boskey ER, Boskey AL. Use of FTIR spectroscopic imaging to identify parameters associated with fragility fracture. J Bone Miner Res. 2009; 24:1565–1571. [PubMed: 19419303]

Inzana JA, Maher JR, Takahata M, Schwarz EM, Berger AJ, Awad HA. Bone fragility beyond strength and mineral density: Raman spectroscopy predicts femoral fracture toughness in a murine model of rheumatoid arthritis. Journal of biomechanics. 2013; 46:723–730. [PubMed: 23261243]

Isaksson H, Turunen MJ, Rieppo L, Saarakkala S, Tamminen IS, Rieppo J, Kroger H, Jurvelin JS. Infrared spectroscopy indicates altered bone turnover and remodeling activity in renal osteodystrophy. Journal of bone and mineral research : the official journal of the American Society for Bone and Mineral Research. 2010; 25:1360–1366.

Iura A, McNerny EG, Zhang Y, Kamiya N, Tantillo M, Lynch M, Kohn DH, Mishina Y. Mechanical Loading Synergistically Increases Trabecular Bone Volume and Improves Mechanical Properties in the Mouse when BMP Signaling Is Specifically Ablated in Osteoblasts. PloS one. 2015; 10:e0141345. [PubMed: 26489086]

Iwasaki Y, Kazama JJ, Yamato H, Fukagawa M. Changes in chemical composition of cortical bone associated with bone fragility in rat model with chronic kidney disease. Bone. 2011; 48:1260–1267. [PubMed: 21397740]

Jepsen KJ. Functional interactions among morphologic and tissue quality traits define bone quality. Clinical orthopaedics and related research. 2011; 469:2150–2159. [PubMed: 21125361]

Kaartinen V, Nagy A. Removal of the floxed neo gene from a conditional knockout allele by the adenoviral Cre recombinase in vivo. Genesis. 2001; 31:126–129. [PubMed: 11747203]

Kamiya N, Kaartinen VM, Mishina Y. Loss-of-function of ACVR1 in osteoblasts increases bone mass and activates canonical Wnt signaling through suppression of Wnt inhibitors SOST and DKK1. Biochem Biophys Res Commun. 2011; 414:326–330. [PubMed: 21945937]

Kamiya N, Kobayashi T, Mochida Y, Yu PB, Yamauchi M, Kronenberg HM, Mishina Y. Wnt inhibitors Dkk1 and Sost are downstream targets of BMP signaling through the type IA receptor (BMPRIA) in osteoblasts. Journal of bone and mineral research : the official journal of the American Society for Bone and Mineral Research. 2010; 25:200–210.

Kamiya N, Ye L, Kobayashi T, Mochida Y, Yamauchi M, Kronenberg HM, Feng JQ, Mishina Y. BMP signaling negatively regulates bone mass through sclerostin by inhibiting the canonical Wnt pathway. Development. 2008a; 135:3801–3811. [PubMed: 18927151]

Kamiya N, Ye L, Kobayashi T, Lucas DJ, Mochida Y, Yamauchi M, Kronenberg HM, Feng JQ, Mishina Y. Disruption of BMP signaling in osteoblasts through type IA receptor (BMPRIA) increases bone mass. Journal of bone and mineral research : the official journal of the American Society for Bone and Mineral Research. 2008b; 23:2007–2017.

Kamiya N, Shuxian L, Yamaguchi R, Phipps M, Aruwajoye O, Adapala NS, Yuan H, Kim HK, Feng JQ. Targeted disruption of BMP signaling through type IA receptor (BMPR1A) in osteocyte suppresses SOST and RANKL, leading to dramatic increase in bone mass, bone mineral density and mechanical strength. Bone. 2016; 91:53–63. [PubMed: 27402532]

Komori T. Regulation of osteoblast differentiation by Runx2. Advances in experimental medicine and biology. 2010; 658:43–49. [PubMed: 19950014]

Li H, Jiang X, Delaney J, Franceschetti T, Bilic-Curcic I, Kalinovsky J, Lorenzo JA, Grcevic D, Rowe DW, Kalajzic I. Immature osteoblast lineage cells increase osteoclastogenesis in osteogenesis imperfecta murine. The American journal of pathology. 2010; 176:2405–2413. [PubMed: 20348238]

Lim J, Shi Y, Karner CM, Lee SY, Lee WC, He G, Long F. Dual function of Bmpr1a signaling in restricting preosteoblast proliferation and stimulating osteoblast activity in mouse. Development. 2016; 143:339–347. [PubMed: 26657771]

Luderer HF, Bai S, Longmore GD. The LIM protein LIMD1 influences osteoblast differentiation and function. Experimental cell research. 2008; 314:2884–2894. [PubMed: 18657804]

Maes C, Kobayashi T, Selig MK, Torrekens S, Roth SI, Mackem S, Carmeliet G, Kronenberg HM. Osteoblast precursors, but not mature osteoblasts, move into developing and fractured bones along with invading blood vessels. Developmental cell. 2010; 19:329–344. [PubMed: 20708594]

Mandair GS, Morris MD. Contributions of Raman spectroscopy to the understanding of bone strength. BoneKEy reports. 2015; 4:620. [PubMed: 25628882]

McBride SH, McKenzie JA, Bedrick BS, Kuhlmann P, Pasteris JD, Rosen V, Silva MJ. Long bone structure and strength depend on BMP2 from osteoblasts and osteocytes, but not vascular endothelial cells. PloS one. 2014; 9:e96862. [PubMed: 24837969]

Miller LM, Little W, Schirmer A, Sheik F, Busa B, Judex S. Accretion of bone quantity and quality in the developing mouse skeleton. Journal of bone and mineral research : the official journal of the American Society for Bone and Mineral Research. 2007; 22:1037–1045.

Mishina Y, Hanks MC, Miura S, Tallquist MD, Behringer RR. Generation of Bmpr/Alk3 conditional knockout mice. Genesis. 2002; 32:69–72. [PubMed: 11857780]

Mishina Y, Starbuck MW, Gentile MA, Fukuda T, Kasparcova V, Seedor JG, Hanks MC, Amling M, Pinero GJ, Harada S, Behringer RR. Bone morphogenetic protein type IA receptor signaling regulates postnatal osteoblast function and bone remodeling. The Journal of biological chemistry. 2004; 279:27560–27566. [PubMed: 15090551]

Morgan S, Poundarik AA, Vashishth D. Do Non-collagenous Proteins Affect Skeletal Mechanical Properties? Calcified tissue international. 2015; 97:281–291. [PubMed: 26048282]

Nakashima K, Zhou X, Kunkel G, Zhang Z, Deng JM, Behringer RR, de Crombrugghe B. The novel zinc finger-containing transcription factor osterix is required for osteoblast differentiation and bone formation. Cell. 2002; 108:17–29. [PubMed: 11792318]

Nilsson A, Ohlsson C, Isaksson OG, Lindahl A, Isgaard J. Hormonal regulation of longitudinal bone growth. European journal of clinical nutrition. 1994; 48(Suppl 1):S150–158. discussion S158–160.

Powles TJ, Hickish T, Kanis JA, Tidy A, Ashley S. Effect of tamoxifen on bone mineral density measured by dual-energy x-ray absorptiometry in healthy premenopausal and postmenopausal women. Journal of clinical oncology : official journal of the American Society of Clinical Oncology. 1996; 14:78–84. [PubMed: 8558225]

Rodda SJ, McMahon AP. Distinct roles for Hedgehog and canonical Wnt signaling in specification, differentiation and maintenance of osteoblast progenitors. Development. 2006; 133:3231–3244. [PubMed: 16854976]

Rux DR, Song JY, Pineault KM, Mandair GS, Swinehart IT, Schlientz AJ, Garthus KN, Goldstein SA, Kozloff KM, Wellik DM. Hox11 Function Is Required for Region-Specific Fracture Repair. Journal of bone and mineral research : the official journal of the American Society for Bone and Mineral Research. 2017; 32:1750–1760.

Shi C, Iura A, Terajima M, Liu F, Lyons K, Pan H, Zhang H, Yamauchi M, Mishina Y, Sun H. Deletion of BMP receptor type IB decreased bone mass in association with compromised osteoblastic differentiation of bone marrow mesenchymal progenitors. Scientific reports. 2016; 6:24256. [PubMed: 27048979]

Soriano P. Generalized lacZ expression with the ROSA26 Cre reporter strain. Nature genetics. 1999; 21:70–71. [PubMed: 9916792]

Stock SR. The Mineral-Collagen Interface in Bone. Calcified tissue international. 2015; 97:262–280. [PubMed: 25824581]

Taylor EA, Lloyd AA, Salazar-Lara C, Donnelly E. Raman and Fourier Transform Infrared (FT-IR) Mineral to Matrix Ratios Correlate with Physical Chemical Properties of Model Compounds and Native Bone Tissue. Applied spectroscopy. 2017; 71:2404–2410. [PubMed: 28485618]

Turunen MJ, Prantner V, Jurvelin JS, Kroger H, Isaksson H. Composition and microarchitecture of human trabecular bone change with age and differ between anatomical locations. Bone. 2013; 54:118–125. [PubMed: 23388419]

Turunen MJ, Saarakkala S, Rieppo L, Helminen HJ, Jurvelin JS, Isaksson H. Comparison between infrared and Raman spectroscopic analysis of maturing rabbit cortical bone. Applied spectroscopy. 2011; 65:595–603. [PubMed: 21639980]

Urist MR. Bone: formation by autoinduction. Science. 1965; 150:893–899. [PubMed: 5319761]

Wallace JM, Ron MS, Kohn DH. Short-term exercise in mice increases tibial post-yield mechanical properties while two weeks of latency following exercise increases tissue-level strength. Calcified tissue international. 2009; 84:297–304. [PubMed: 19283427]

Wallace JM, Rajachar RM, Allen MR, Bloomfield SA, Robey PG, Young MF, Kohn DH. Exercise-induced changes in the cortical bone of growing mice are bone- and gender-specific. Bone. 2007; 40:1120–1127. [PubMed: 17240210]

Wang L, Mishina Y, Liu F. Osterix-Cre transgene causes craniofacial bone development defect. Calcified tissue international. 2015; 96:129–137. [PubMed: 25550101]

Zhang J, Niu C, Ye L, Huang H, He X, Tong WG, Ross J, Haug J, Johnson T, Feng JQ, Harris S, Wiedemann LM, Mishina Y, Li L. Identification of the haematopoietic stem cell niche and control of the niche size. Nature. 2003; 425:836–841. [PubMed: 14574412]

Zhang Y, McNerny EG, Terajima M, Raghavan M, Romanowicz G, Zhang Z, Zhang H, Kamiya N, Tantillo M, Zhu P, Scott GJ, Ray MK, Lynch M, Ma PX, Morris MD, Yamauchi M, Kohn DH, Mishina Y. Loss of BMP signaling through BMPR1A in osteoblasts leads to greater collagen cross-link maturation and material-level mechanical properties in mouse femoral trabecular compartments. Bone. 2016; 88:74–84. [PubMed: 27113526]

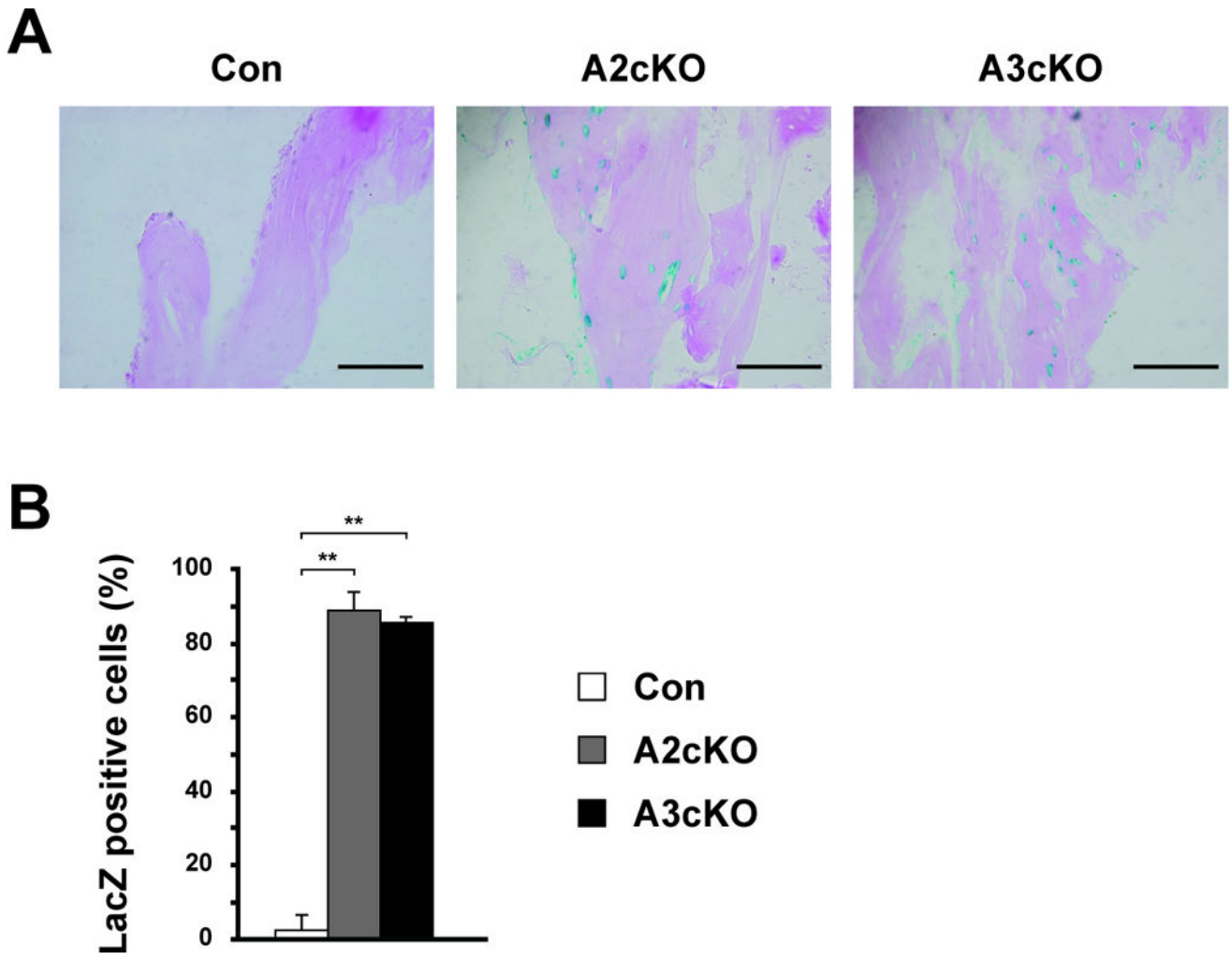

Fig. 1.

Evidence of gene deletion by X-gal staining at 3 months of age. (A) Representative images of X-gal staining, showing proximal tibiae of control, A2cKO and A3cKO mice. Bar = 50 μm. (B) Proportion of LacZ positive cells in osteoblast lineage per high magnification field (40×). For each group, n = 3. *: $p < 0.05$; **: $p < 0.01$. con: control; A2cKO: *Acvr1* conditional knockout; A3cKO: *Bmpr1a* conditional knockout.

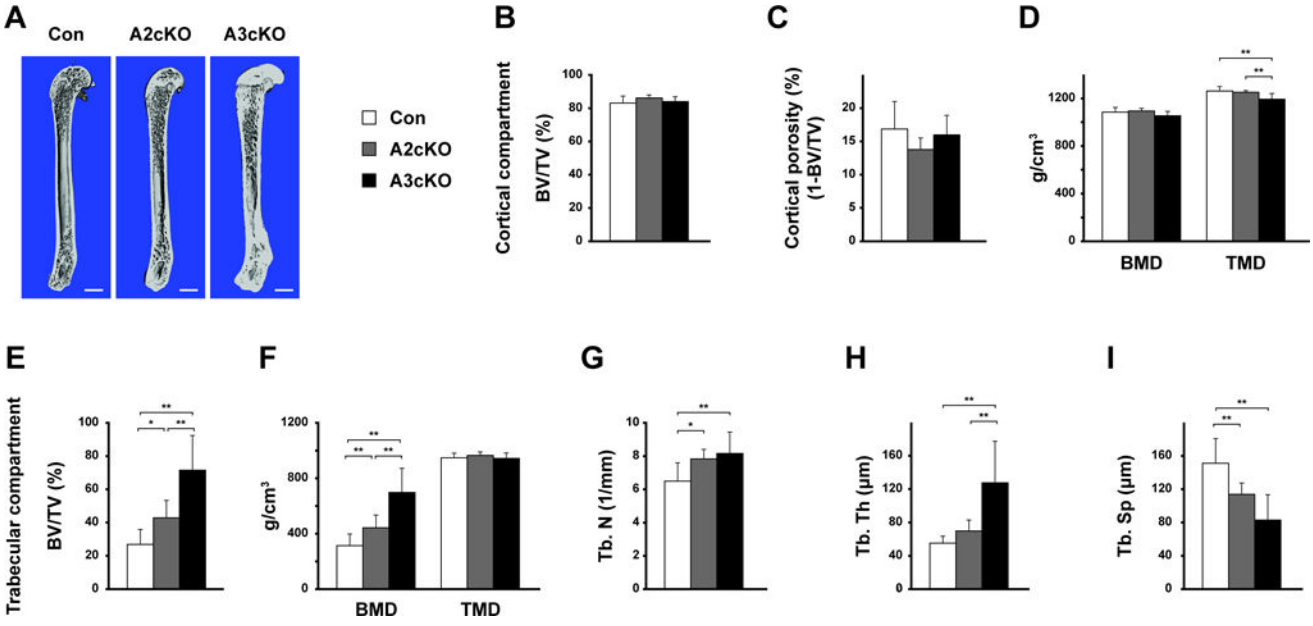

Fig. 2.

Micro-CT results show greater bone mass in A2cKO and A3cKO male mice at 3 months of age, and A3cKO showed significantly more bone mass than A2cKO. (A) Representative images of micro-CT scanning. Bar = 1 mm. (B–D) Cortical parameters were determined by micro-CT for the femurs from 3-month-old male mice: (B) bone volume fraction (bone volume/tissue volume, BV/TV); (C) cortical porosity; (D) bone mineral density (BMD) and tissue mineral density (TMD). (E–I) Trabecular parameters: (E) BV/TV; (F) BMD and TMD; (G) trabecular number (Tb. N); (H) trabecular thickness (Tb. Th); (I) trabecular separation (Tb. Sp). For control and A2cKO group, n = 10; for A3cKO, n = 9. *: $p < 0.05$; **: $p < 0.01$. con: control; A2cKO: *Acvr1* conditional knockout; A3cKO: *Bmpr1a* conditional knockout.

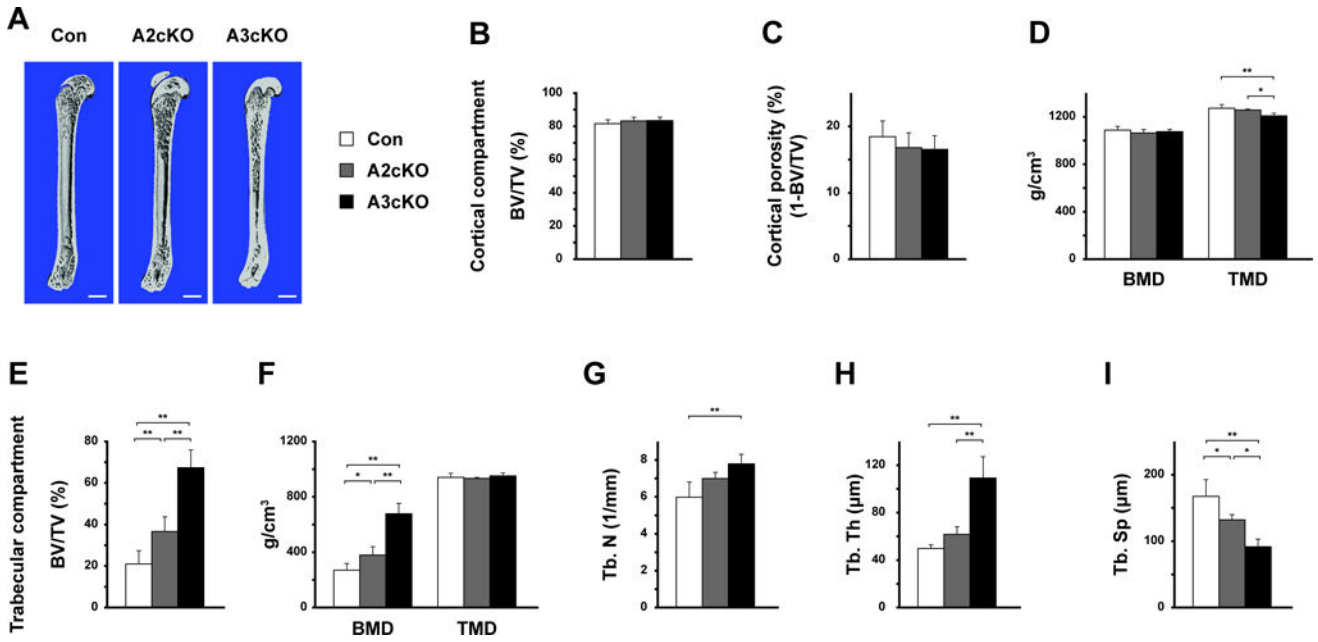

Fig. 3.

Micro-CT results show increased bone mass in both conditional knockout mice of 3 months old female, and A3cKO showed significantly more bone mass compared with A2cKO. (A) Representative images of micro-CT scanning. Bar = 1 mm. (B–D) Cortical parameters were determined by micro-CT for the femurs from 3-month-old female mice: (B) bone volume fraction (bone volume/tissue volume, BV/TV); (C) cortical porosity; (D) bone mineral density (BMD) and tissue mineral density (TMD). (E–I) Trabecular parameters: (E) BV/TV; (F) BMD and TMD; (G) trabecular number (Tb. N); (H) trabecular thickness (Tb. Th); (I) trabecular separation (Tb. Sp). For control group, n = 12; for A2cKO, n = 4; for A3cKO, n = 10. *: $p < 0.05$; **: $p < 0.01$. con: control; A2cKO: *Acvr1* conditional knockout; A3cKO: *Bmpr1a* conditional knockout.

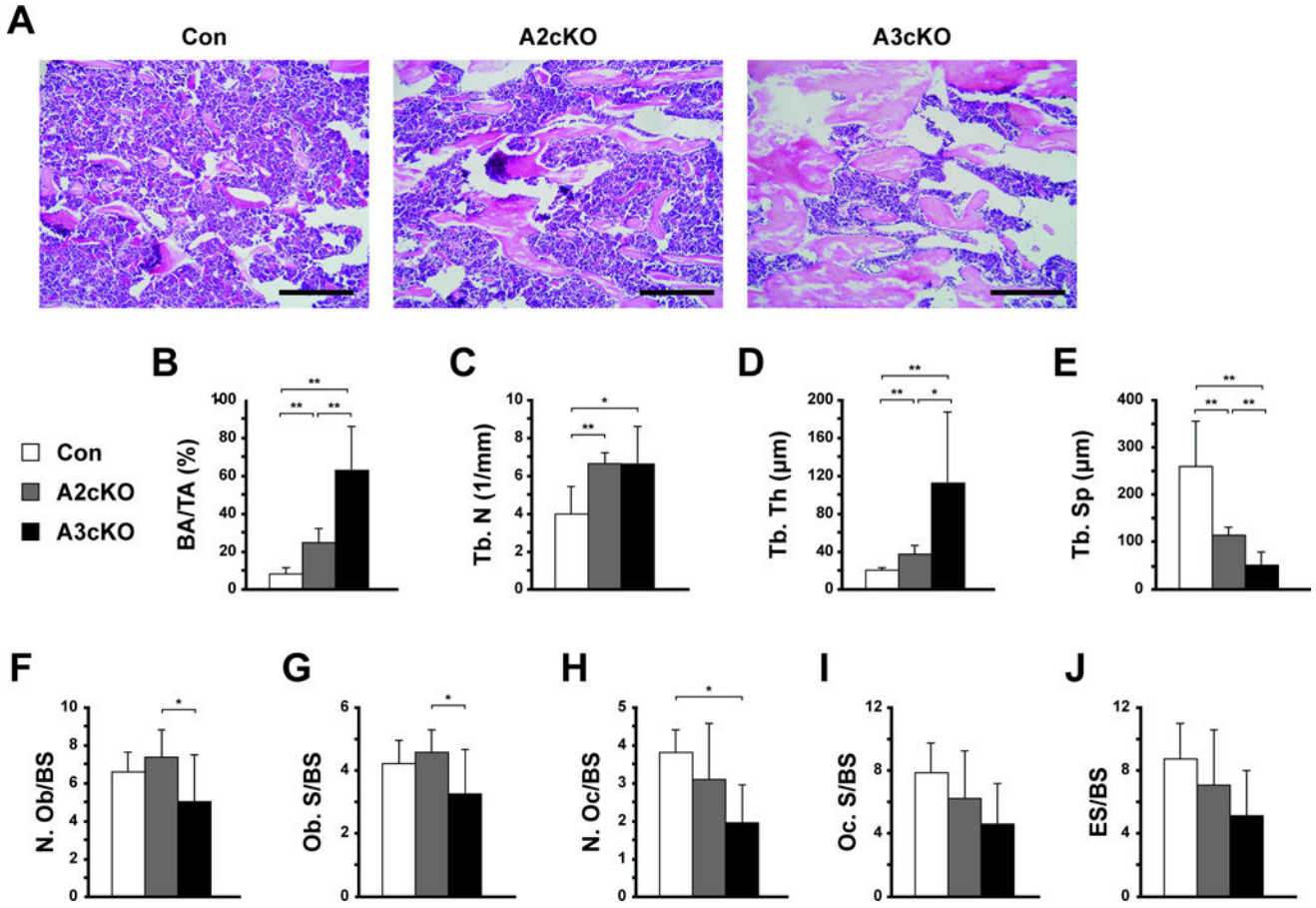

Fig. 4.

Histomorphometric analysis of the distal femur of 3-month-old male mice. (A) Representative images of histology. Bar = 200 μm. (B) Trabecular bone area/tissue area (BA/TA). (C) Tb. N. (D) Tb. Th. (E) Tb. Sp. (F) Osteoblast number per bone surface (N. Ob/BS). (G) Osteoblast surface per bone surface (Ob. S/BS). (H) Osteoclast number per bone surface (N. Oc/BS). (I) Osteoclast surface per bone surface (Oc. S/BS). (J) Eroded surface per bone surface (ES/BS). For each group, n = 3. *: $p < 0.05$; **: $p < 0.01$. con: control; A2cKO: *Acvr1* conditional knockout; A3cKO: *Bmpr1a* conditional knockout.

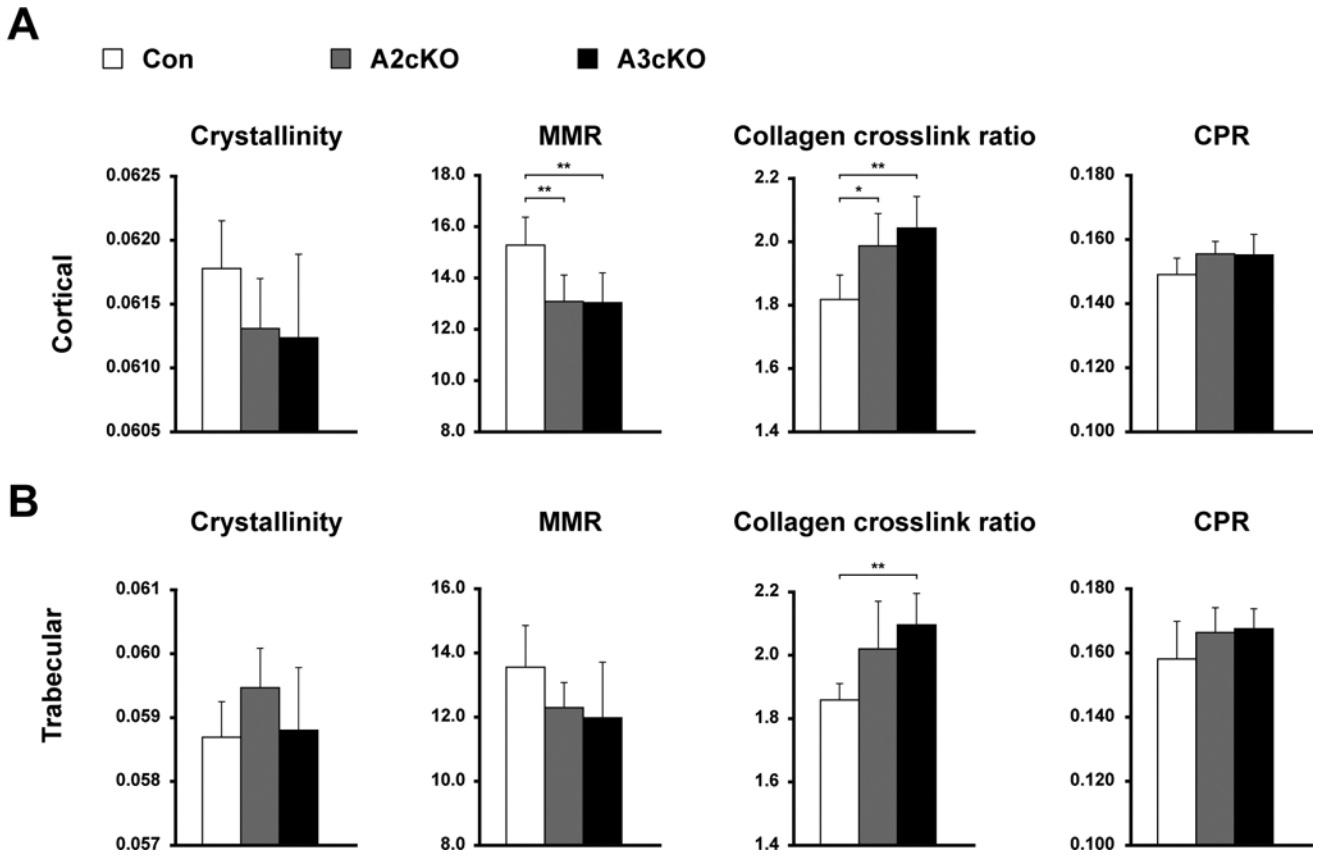

Fig. 5.

Conditional knockout male mice show altered bone composition by Raman spectroscopy. Raman spectroscopy measurements of mineral crystallinity, mineral/matrix ratio (MMR), collagen crosslink ratio, and carbonate/phosphate ratio (CPR) at (A) cortical and (B) trabecular compartments. For each group, n = 6. Statistical analysis was performed between those that were adequately powered (80%, a = 0.05). *: $p < 0.05$; **: $p < 0.01$. con: control; A2cKO: *Acvr1* conditional knockout; A3cKO: *Bmpr1a* conditional knockout.

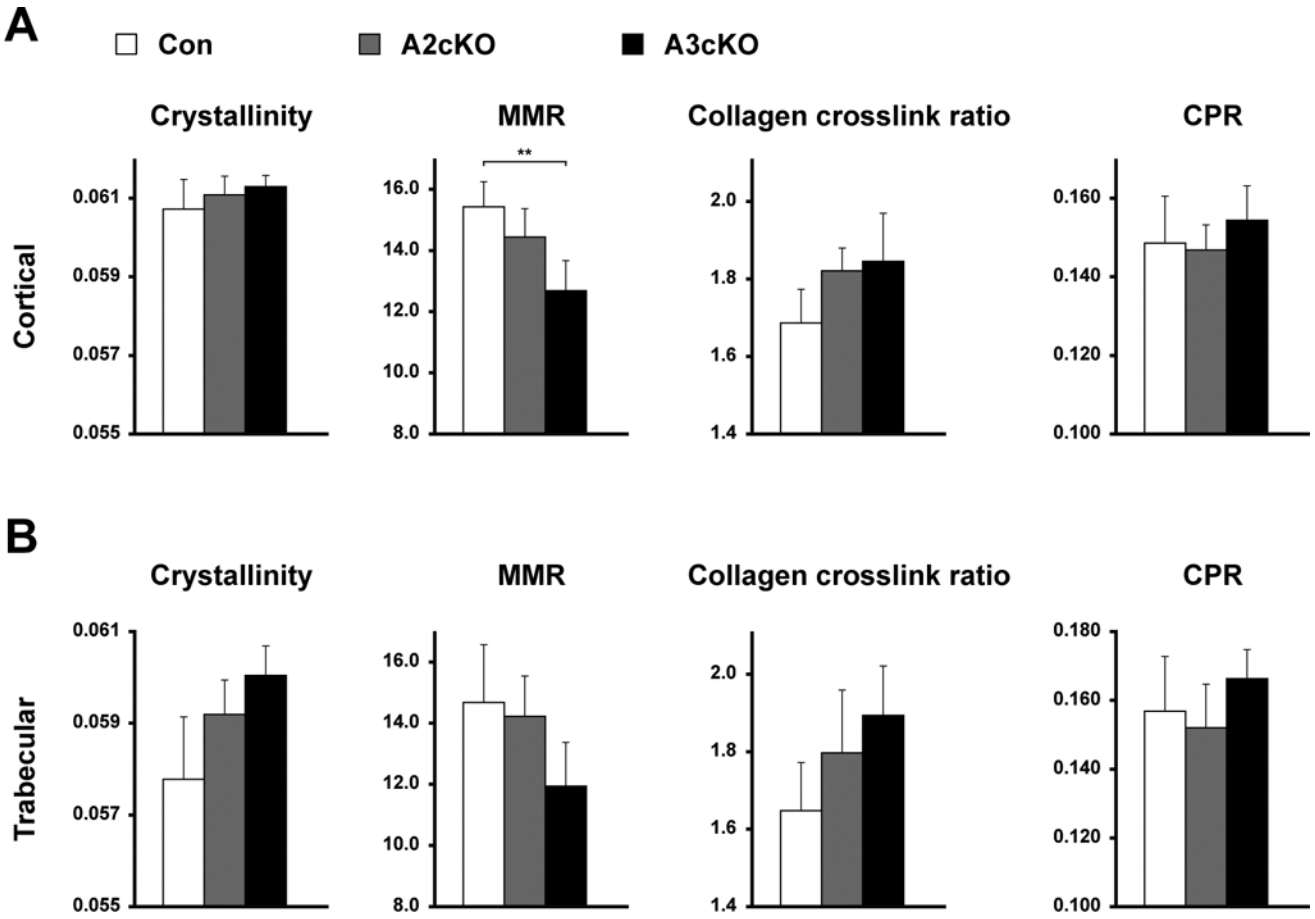

Fig. 6.

Conditional knockout female mice show altered bone composition by Raman spectroscopy. Raman spectroscopy measurements of mineral crystallinity, mineral/matrix ratio (MMR), collagen crosslink ratio, and carbonate/phosphate ratio (CPR) at (A) cortical and (B) trabecular compartments. For each group, n = 4. Statistical analysis was performed between those that are adequately powered (80%, a = 0.05). **: $p < 0.01$. con: control; A2cKO: *Acvr1* conditional knockout; A3cKO: *Bmpr1a* conditional knockout.

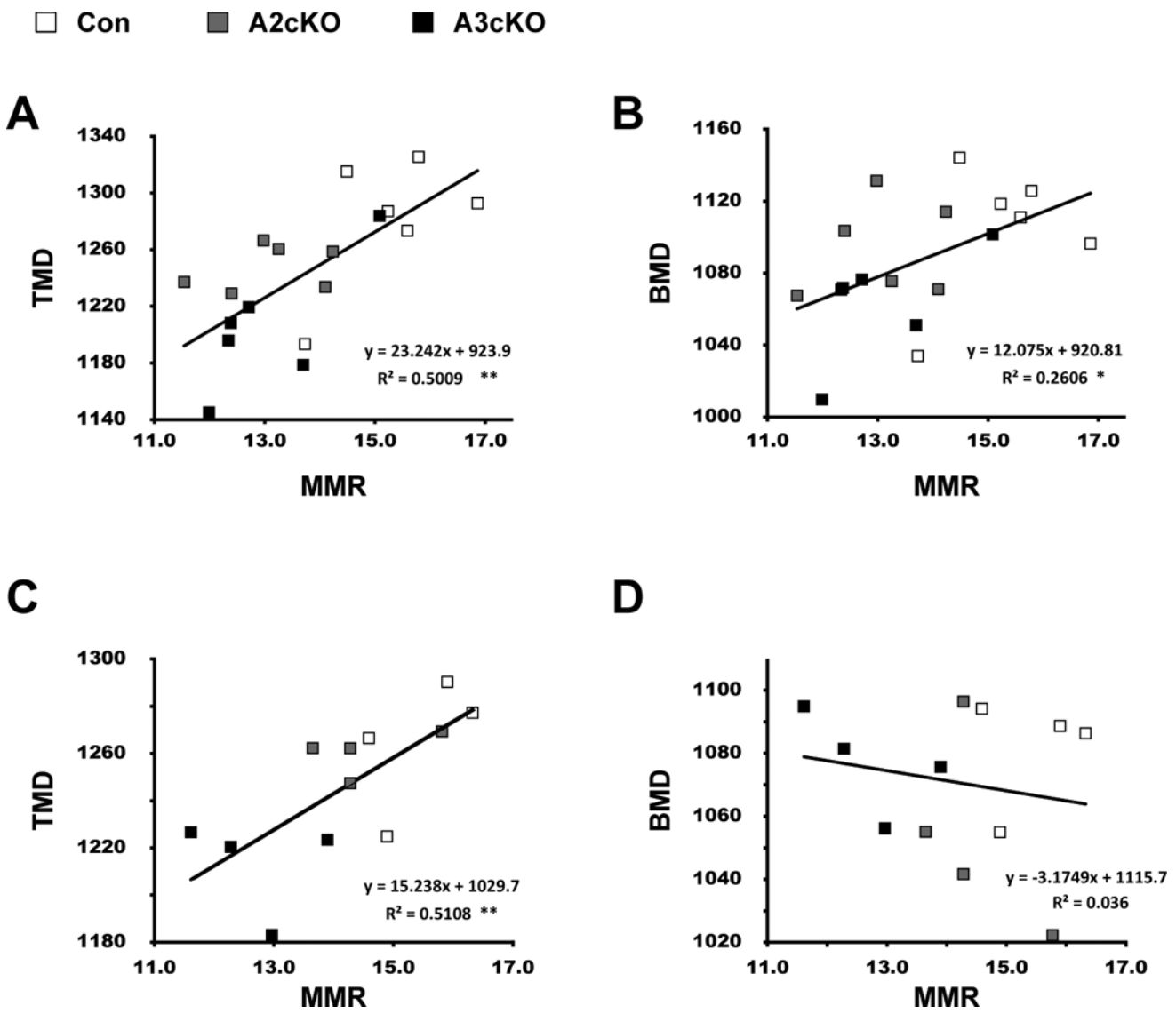

Fig. 7.

Correlation between TMD vs. MMR (A) and BMD vs. MMR (B) in males and TMD vs. MMR (C) and BMD vs. MMR (D) in females were performed. R^2 values were obtained respectively. *: $p < 0.05$; **: $p < 0.01$. con: control; A2cKO: *Acvr1* conditional knockout; A3cKO: *Bmpr1a* conditional knockout.